...

Matt Ellis

A dissertation submitted in partial fulfillment
of the requirements for the degree of
Doctor of Philosophy
of
University College London.

Department of Physics and Astronomy
University College London

January 12, 2021

I, Matt Ellis, confirm that the work presented in this thesis is my own. Where information has been derived from other sources, I confirm that this has been indicated in the work.

Abstract

My research is about stuff.

It begins with a study of some stuff, and then some other stuff and things.

There is a 300-word limit on your abstract.

Acknowledgements

Acknowledge all the things!

Contents

List of Figures

List of Tables

Chapter 1

Introduction

1.1 Charge Transport in Organic Semiconductors

1.1.1 Organic Semiconductors

Conductive polymers were first discovered in 1977 by Shirakawa et al[1,2] for which they were awarded the Nobel prize in Chemistry. Recently these materials have become ubiquitous in many technologies, such as in organic photovoltaic cells[3], organic field-effect transistors (OFET)[4] and organic light-emitting diodes (OLED)[5]. While the other two technologies lag behind their inorganic counterparts, uptake of OLED screens is becoming ubiquitous -especially in the smartphone and television market due to their flexibility, better colour representation and lower energy consumption than standard backlit LCD displays. OLEDs have also found uses in lighting with their efficiency rivalling that of fluorescent tubes[6,7]. Although, industry has made large strides in fabricating and using these materials the exact nature of the charge transport is still poorly understood. Traditional theories (such as hopping and band transport) aren't applicable to many relevant materials[8–12] as charge transfer dynamics lies in an intermediate region where the polaron is neither fully localised or delocalised. This is due to crystals typically being formed of organic molecules weakly held together by Van der Waals (VDW) forces rather than strong covalent bonds. This allows molecules to fluctuate about their lattice sites and introduces a disorder that doesn't appear in inorganic crystals.

In order to properly quantify the performance of organic semiconductors a key prop-

erty is the charge carrier mobility. Typically, charge carrier mobilities in 'good' organic semiconductors (OSCs) fall between 1-10 $cm^2V^{-1}s^{-1}$ [13]. Though higher mobilities, in pure crystals such as Rubrene, have been recorded in the range 15-20+ $cm^2V^{-1}s^{-1}$ [14,15]. This is beyond the range of hopping model validity ($\sim$1 $cm^2V^{-1}s^{-1}$) and below that of band theory ($>$ 50 $cm^2V^{-1}s^{-1}$) [12]. In this intermediate regime the charge carriers are typically not completely delocalised at the valence band edges (band regime) or localised to a single site/molecule (hopping regime) but delocalised over a few/tens of molecules [16]. Without any analytic approaches currently being valid in this regime many atomistic computational approaches have been developed to investigate the underlying charge transport mechanisms [17].

1.2 Atomistic Simulations of Nonadiabatic Processes

In simulating processes involving electronic transfers a key approximation used in conventional molecular dynamics (MD) breaks down. That is the Born-Oppenheimer or adiabatic approximation [18]. This approximation, relied upon for almost a century [19], hinges on the fact that nuclei are much more massive than electrons and are approximately stationary with respect to electron movement [20]. This results in nuclear evolution that is governed by a single, adiabatic, potential energy surface. However, in many interesting processes, such as the proton coupled electron transfer in photosynthesis and respiration [21–23], non-radiative decay and photochemical processes, electronic transitions between adiabatic potential energy surfaces occur [24]. Simulating these processes requires non-adiabatic molecular dynamics (NAMD) techniques to be developed, to correctly capture dynamical properties.

There have been many techniques proposed for use in NAMD such as the quantum classical Louiville equation [25], multiple spawning [26] or nonadiabatic Bohmian dynamics [27]. However, two of the most popular are trajectory surface hopping [28] and mean-field approaches [29]. This is probably due to their relative simplicity to implement, efficiency for

large systems and proven efficacy in a wide variety of situations[30]. In these approaches the general aim is to treat as much of the system as possible with (computationally cheaper) classical mechanics. While handling all necessary parts with quantum mechanics[31]. In Surface Hopping, Ehrenfest and Coupled-Trajectory Mixed Quantum-Classical molecular dynamics (CTMQC) one treats the nuclear subsystem classically and the electronic one quantum mechanically. The nuclei are normally propagated using a velocity verlet algorithm according to Newton's laws and electrons using a fourth order Runge Kutta algorithm according to the time-dependent Schrödinger equation. The wavefunction is normally expanded as a linear combination of adiabatic or diabatic states. The nuclei and electrons can also interact. Taking account of this interaction is where these techniques differ. No one technique is perfect, the issues for surface hopping and Ehrenfest are well documented and have been discussed in detail[32–36]. CTMQC is a fairly new technique and its issues are still mostly unknown. In this document I will discuss CTMQC in depth and present results from my own implementation of it as well as presenting its drawbacks. I will also compare these results to Ehrenfest and Trajectory Surface Hopping (TSH).

1.2.1 Surface Hopping and Ehrenfest Dynamics

An important technique in the field of mixed quantum classical nonadiabatic molecular dynamics is Ehrenfest dynamics. Assuming we treat the nuclei classically the Ehrenfest equations can be rigorously derived from the electronic Schrödinger equation. This is done by assuming that the nuclei's motion is provided by a single population weighted average potential energy surface. This average is taken from the adiabatic potential energy surfaces (eigenvalues of the Hamiltonian) where weights are provided by the populations of each adiabatic state. This effective potential energy surface is shown in fig 1.1. In this way the electronic

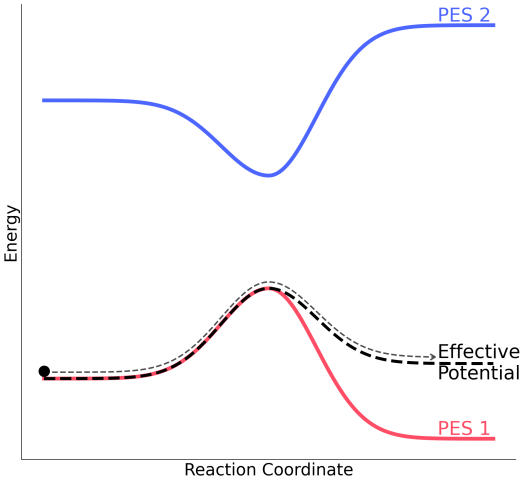

Figure 1.1: An example of a typical Ehrenfest simulation near an avoided crossing. The black lines represent the adiabatic potential energy surface due to the ground (PES 1) and excited (PES 2) state. The red line represents the population weighted average potential the nuclei travel on.

subsystem influences the propagation of the nuclei. The propagation of the forces and the electrons are controlled by equations (1.1) and (1.2).

$$F_{\nu}^{Ehren} = \sum_{i}^{N_{st}} |C_i|^2 \nabla_{\nu} E_i + \sum_{i,j}^{N_{st}} C_i^* C_j (E_j - E_i) \mathrm{d}_{ij,\nu} \tag{1.1}$$

$$i\hbar \dot{\vec{C}}_m = C_m E_m - i\hbar \sum_{n}^{N_{st}} C_n d_{mn}^{ad} \tag{1.2}$$

In the above equations C_i is the adiabatic expansion coefficient for state i, E_m is the energy of adiabatic state m, $\mathrm{d}_{mn,\nu}^{ad}$ is the nonadiabatic coupling (in the adiabatic basis) between states m and n for atom ν. The d_{mn}^{ad} are the nonadiabatic coupling elements expressed in the adiabatic basis. Although the Ehrenfest method has been applied with success in many systems[37–39] it has a number of key shortcomings. Namely, its inability to capture the branching of the nuclear wavefunction as propagation occurs on only a single potential energy surface and its poor account of the decoherence of the electronic and nuclear subsystem after an avoided crossing. Ehrenfest also violates detailed balance by populating all adiabatic states evenly[18,40]. In the limit of infinite states this results in infinite electronic temperature[41]. Possibly the most popular technique in NAMD is trajectory surface hopping. In trajectory surface hopping the shape of the potential energy surface is determined by a series of discrete stochastic hops between adiabatic potential energy surfaces[40]. See fig 1.2. The probability of these hops is determined by the non-adiabatic coupling between states. A swarm of trajectories are used and the probability a hop (non-adiabatic coupling) determines how many of these change state. The nuclear dynamics are dictated by the shape of the energy surface they are travelling on. This method can capture the branching of nuclear wavepacket unlike Ehrenfest. However, it still suffers from a number of issues. The original 'fewest switches surface hopping' proposed by John Tully suffered from bad overcoherence of the nuclear and electronic subsystems. That is the electronic and nuclear motion was coupled long after the region of high non-adiabatic coupling (crossing region). The fact that the hops are instant leads to discontinuities and methods need to

be implemented to fix these such as velocity re-scaling. Finally, perhaps the most important shortcoming is that this technique has not been derived from first principles and cannot be guaranteed to work generally. These problems have lead to a number of other techniques being developed. One of these, CTMQC, is the subject of this report.

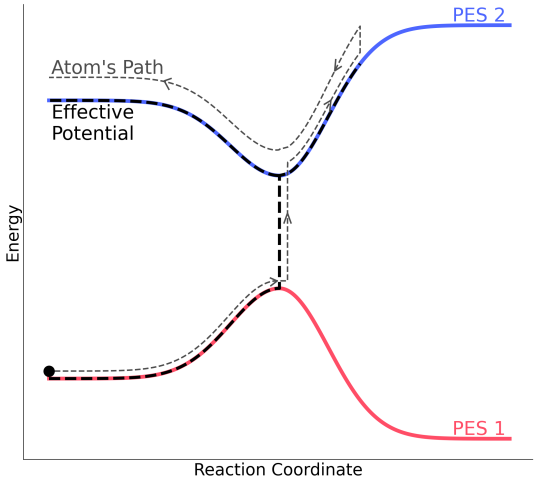

Figure 1.2: An example of a typical Surface Hopping simulation near an avoided crossing. The black lines represent the adiabatic potential energy surface due to the ground (PES 1) and excited (PES 2) state. The red line represents the discontinuous effective potential the nuclei travel on.

Chapter 2

CTMQC applied to the Tully Models

The Tully models, first proposed by John Tully in 1990[42], are a collection of simple 1 dimensional model systems. They were designed to be simple enough to obtain accurate quantum results to benchmark new nonadiabatic molecular dynamics (NAMD) methods against. Originally there were 3, 1 dimensional, 1 atom models. However, in this work an extra model has been introduced with parameters taken from Gossel, 18[43]. This is to allow a full comparison of my implementation of CTMQC with the literature. In this chapter my implementation of CTMQC will be tested using these model systems and by comparing my results with those in the literature.

In each of the Tully models the (diabatic) Hamiltonian is a function of nuclear positions and is a 2×2 matrix that takes the form:

$$\hat{H} = \frac{\hat{P}^2}{2M} + \begin{pmatrix} H_{11}(\mathbf{R}) & H_{12}(\mathbf{R}) \\ H_{21}(\mathbf{R}) & H_{22}(\mathbf{R}) \end{pmatrix} \tag{2.1}$$

The nuclear mass has been set to 2000 a.u.. This was set to be very close to the proton's mass of 1836 a.u. so we can expect significant quantum effects that classical theory couldn't replicate. The values of the Hamiltonian matrix elements are set to produce systems that resemble common features in a typical nonadiabatic simulation such as avoided crossings and regions of extended coupling. The parameters used in each systems' Hamiltonian where taken from Gossel, 18[43] in order to compare the 2 implementations. These can be found in appendix A.

In order to propagate dynamics in the adiabatic basis we need to calculate various quantities from the hamiltonian at each timestep. These are, for Ehrenfest, the (adiabatic) nonadiabatic coupling vector ($\mathbf{d}_{lk}^{(I)}$) and the adiabatic energies ($E_l^{(I)}$). In the full CTMQC simulations we must also calculate the adiabatic momentum term $\mathbf{f}_l^{(I)}$ from the Hamiltonian. The adiabatic energies are the eigenvalues of the Hamiltonian. The adiabatic NACV can be calculated via an (explicit Euler) finite difference method and equation (2.2) below.

$$\mathbf{d}_{lk}^{(I)} = \langle \psi_l^{(I)} | \nabla \psi_k^{(I)} \rangle \tag{2.2}$$

Where $\psi_l^{(I)}$ is the adiabatic electronic basis function for adiabatic state l. This is given by the eigenvector of the Hamiltonian, on replica I, corresponding to state l. Illustrations of these 2 properties can be found below in fig 2.1 for each of the 4 models systems.

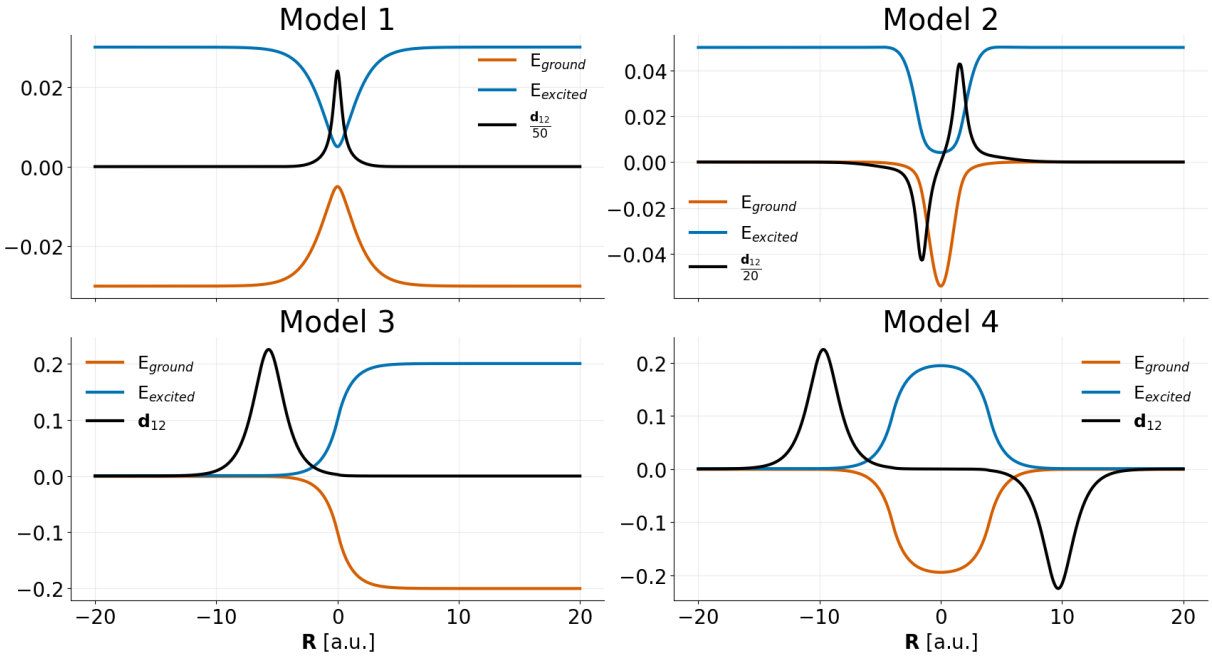

Figure 2.1: Adiabatic potential energy surfaces (orange and blue) and element 1, 2 of the nonadiabatic coupling vector (black) for the 4 model systems. For parameters see appendix A.

In order to initialise the simulations coordinates and velocities were sampled from the Wigner phase-space distribution of a gaussian nuclear wavepackets given by equation (2.3). A derivation of this can be found in appendix B. The nuclear positions/velocities were then propagated using a velocity verlet algorithm and the adiabatic expansion coefficients were propagated using a 4^{th} order Runge-Kutta method.

$$\chi(R,0) = \frac{1}{(\pi\mu^2)^{\frac{1}{4}}} e^{-\frac{(R-R_0)^2}{2\mu^2} + \mathrm{i}k_0(R-R_0)} \tag{2.3}$$

The adiabatic coefficients were initialised purely on the ground state and the initial width of the nuclear wavepacket was set to $\mu = \sqrt{2}$ bohr. 2 values of initial momenta k_0 were chosen for each model, 1 low value and another higher one. Full details of all input parameters can be found in appendix A. I have implemented a serial version of CTMQC acting on Tully's toy model systems and real molecular systems using couplings derived from the analytic overlap method[44] within the software package CP2K[45] and for Tully's model systems as standalone python code. These are accessible publicly via github repositories at: github.com/95ellismle.

2.1 Testing My Implementation

The motivation behind implementing CTMQC for the Tully models was to serve as a verifiable base for later extensions, such as integrating CTMQC within the fragment-orbital based (FOB)[46] framework which will be discussed in a later chapter[?] . Using such simple systems will also help to clarify how each new parameter works and make testing and debugging easier. As well as many numerical tests on individual terms in the equations, I have implemented some physical tests on the overall system dynamics. In this section, I will outline the key tests I have performed on both the Ehrenfest and full CTMQC parts of the equations. These are: verifying we obtain Rabi oscillation in the limit of fixed nuclear geometries, checking energy and the norm of the wavefunction is conserved and verifying the time-derivative of the sum over trajectories of adiabatic populations is 0.

2.1.1 Rabi Oscillation

...

2.1.2 Energy Conservation

...

2.1.3 Norm Conservation

In appendix ?? it is shown that the norm of the adiabatic coefficients

2.1.4 Time Derivative of Trajectory-Sum of Adiabatic Populations

...

Chapter 3

CTMQC applied to molecular systems

Chapter 4

Extending surface hopping for larger systems

Fragment-orbital based surface hopping (FOB-SH) is a technique developed within the Blumberger group[46] designed to simulate large molecular systems. It has had much success in the study of organic crystalline materials[16,47]. Most notably the electron/hole mobilities of a variety of common organic semi-conducting materials were measured within a factor of 2 of experimental measurements. However, in order to study very large amorphous and semi-crystalline systems some more memory/computation optimisations were required and electrostatic interactions (which weren't important in previous systems) needed to be accounted for. In this chapter I outline some minor improvements I implemented within the surface hopping code as well as the method used to implement the electrostatic interactions.

4.1 Code Optimisations

Chapter 5

Charge transfer in amorphous systems

Although it is important to know the maximum bound on the mobility of the charge carrier in a perfect crystal of an organic semiconductor, in reality it is very difficult to control defect formation in OSs[48?] . This is due to van der Waals forces only weakly holding molecules at lattice sites, allowing molecules greater freedom than in traditional inorganic crystal, and increasing the chance of defect formation which can trap/scatter charge carriers reducing overall mobility. This means it is important to investigate and characterise charge transport properties for not just perfectly crystalline OSs but also those that show a range of amorphicity.

The molecule chosen to investigate amorphous films was pentacene. This molecule is a popular organic semiconductor and the subject of much research due to its high field effect mobility[49], use in device applications[50] and, more recently, the use of functionalization to alter device properties[51,52]. The pentacene molecule consists of 5 joined benzene rings (36 atoms) and crystals typically pack with a herringbone motif as shown in figure 5.1.

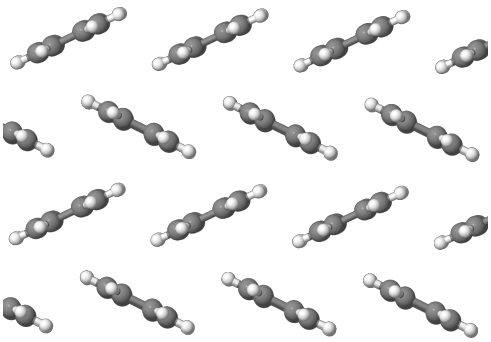

Figure 5.1: An example of the herringbone packing typically found in Pentacene crystals

5.1 Creating Amorphous Pentacene

In order to create the amorphous pentacene systems

a melt-quench technique was used...

Chapter 6

Extending surface hopping with electrostatics

6.1 Electrostatics interaction within FOB-SH

FOB-SH is a variant of Tully's original fewest switches surface hopping (ref John Tully 1990 original surface hopping paper). The electron and nuclear dynamics are dictated by the Hamiltonian, where the spatial derivative of the diagonal elements (site-energies) give the nuclear forces which come from a classical forcefield and the off-diagonal elements (electron couplings) are proportional to the overlap of the diabatic wavefunctions. Each site-energy, $H_{\gamma\gamma}$, is defined as the potential energy of the system where the excess charge is localised on a single molecule, γ. The input parameters such as the charge distribution or the strength of the bonds are different for molecule γ than the other molecules, resulting in different forces/potentials. The different potentials from each permutation of the charge state are saved as the site-energies, the forces are saved in a different array of size $(N_{states}, N_{atoms}, 3)$. To implement electrostatic interactions the potential and the forces within the surface hopping framework will have to be altered.

To calculate the electrostatic contribution from each atom to the forces and potential the standard Ewald method was chosen, with some additional tricks to reduce the computational cost. The Ewald method, first published by Paul Ewald in 1921 (NEED REF), is a near ubiquitous method used to evaluate the potential and forces from a set of point charges. This is equivalent to carrying out the much slower to converge (NEED REF) and conditionally convergent traditional coulomb sum. The Ewald method relies

on separating the traditional coulomb summation into 2 quickly converging parts; a long range term and short range term. The short range term is carried out in real space and the long range term is carried out in carried out in reciprocal space

Chapter 7

General conclusions

Appendix A

Tully Model Paramters

A.1 Model 1 -Single Avoided Crossing

Hamiltonian Paramters:

$$H_{11}(\mathbf{R}) = A \tanh(B\mathbf{R})$$
$$H_{12}(\mathbf{R}) = Ce^{-D\mathbf{R}^2}$$
$$H_{21}(\mathbf{R}) = H_{12}(\mathbf{R})$$
$$H_{22}(\mathbf{R}) = -H_{11}(\mathbf{R})$$

Where A = 0.03, B = 0.4, C = 0.005 and D = 0.3

Quantity	Value	Unit
Initial Position	-20	a.u.
Initial Velocities	15.0, 25.0	a.u.
Initial Adiab Pop	ground state	-
Simulation Time	6000, 4000	a.u.
$\sigma_v^{(I)}$	0.5	a.u.
M (σ constant)	40	-
$\Delta t_{\text{nuclear}}$	0.1	fs
$\Delta t_{\text{electonic}}$	0.01	fs
$\frac{\delta \mathbf{R}_{lk,v}^{(I)}}{\delta t}$ threshold	0.15	a.u.
N_{rep}	200	-

A.2 Model 2 -Dual Avoided Crossing

Hamiltonian Paramters:

$$H_{11}(\mathbf{R}) = 0$$
$$H_{12}(\mathbf{R}) = Ce^{-D\mathbf{R}^2}$$
$$H_{21}(\mathbf{R}) = H_{12}(\mathbf{R})$$
$$H_{22}(\mathbf{R}) = -Ae^{-B\mathbf{R}^2} + E$$

Where A = 0.1, B = 0.28, C = 0.015, D = 0.06 and E = 0.05

Quantity	Value	Unit
Initial Position	-8	a.u.
Initial Velocities	16.0, 30.0	a.u.
Initial Adiab Pop	ground state	-
Simulation Time	2500, 1500	a.u.
$\sigma_\nu^{(I)}$	0.5	a.u.
M (σ constant)	40	-
$\Delta t_{\text{nuclear}}$	0.1	fs
$\Delta t_{\text{electonic}}$	0.01	fs
$\frac{\delta \mathbf{R}_{lk,\nu}^{(I)}}{\delta t}$ threshold	0.15	a.u.
N_{rep}	200	-

A.3 Model 3 -Extended Coupling

Hamiltonian Paramters:

$$H_{11}(\mathbf{R}) = A$$
$$H_{12}(\mathbf{R}) = \begin{cases} Be^{C\mathbf{R}}, & R \leq 0 \\ B(2 - e^{-C\mathbf{R}}), & R > 0 \end{cases}$$
$$H_{21}(\mathbf{R}) = H_{12}(\mathbf{R})$$
$$H_{22}(\mathbf{R}) = -H_{11}(\mathbf{R})$$

Where A = 6×10^{-4}, B = 0.1 and C = 0.9

Quantity	Value	Unit
Initial Position	-15	a.u.
Initial Velocities	10, 30	a.u.
Initial Adiab Pop	ground state	-
Simulation Time	5000, 1500	a.u.
$\sigma_\nu^{(I)}$	0.5	a.u.
M (σ constant)	40	-
$\Delta t_{\text{nuclear}}$	0.1	fs
$\Delta t_{\text{electonic}}$	0.01	fs
$\frac{\delta \mathbf{R}_{lk,\nu}^{(I)}}{\delta t}$ threshold	0.15	a.u.
N_{rep}	200	-

A.4 Model 4 -Dual Arch

Hamiltonian Paramters:

$$H_{11}(\mathbf{R}) = A$$

$$H_{12}(\mathbf{R}) = \begin{cases} B\left[-e^{C(\mathbf{R}-D)} + e^{C(\mathbf{R}+D)}\right] & R \leq -D \\ B\left[e^{-C(\mathbf{R}-D)} - e^{-C(\mathbf{R}+D)}\right] & R \geq D \\ B\left[2 - e^{C(\mathbf{R}-D)} - e^{-C(\mathbf{R}+D)}\right] & -D < R < D \end{cases}$$

$$H_{21}(\mathbf{R}) = H_{12}(\mathbf{R})$$

$$H_{22}(\mathbf{R}) = -H_{11}(\mathbf{R})$$

Where A = 6×10^{-4}, B = 0.1 and C = 0.9

Quantity	Value	Unit
Initial Position	-20	a.u.
Initial Velocities	10, 40	a.u.
Initial Adiab Pop	ground state	-
Simulation Time	6000, 2000	a.u.
$\sigma_{\nu}^{(I)}$	0.5	a.u.
M (σ constant)	40	-
$\Delta t_{\text{nuclear}}$	0.1	fs
$\Delta t_{\text{electonic}}$	0.01	fs
$\frac{\delta \mathbf{R}_{Ik,\nu}^{(I)}}{\delta t}$ threshold	0.15	a.u.
N_{rep}	200	-

Appendix B

Wigner Distribution Derivation

The nuclear wavepacket (at time 0) is given by:

$$\chi(R) = \frac{1}{(\pi\mu^2)^{\frac{1}{4}}} e^{-\frac{(R-R_0)^2}{2\mu^2} + ik_0(R-R_0)} \tag{B.1}$$

The Wigner quassiprobability function for momentum and position (p, R) is given by:

$$W(p,R) = \frac{1}{\pi\hbar} \int_{-\infty}^{\infty} \chi^*(R+y)\chi(R-y)e^{\frac{2ipy}{\hbar}} dy \tag{B.2}$$

However, both Ehrenfest and CTMQC require atomic positions as input so we must extract the position and velocity probability densities from this. We get these from the marginal integrals of the Wigner distribution i.e.

$$|f(R)|^2 = \int_{-\infty}^{\infty} W(R,p)dp \tag{B.3}$$

$$|f(p)|^2 = \int_{-\infty}^{\infty} W(R,p)dR \tag{B.4}$$

In order to calculate these marignal integrals we must first crunch through the maths of equation (B.2). Substituting eq (B.1) into (B.2):

$$W(p,R) = \frac{1}{\pi\hbar} \int_{-\infty}^{\infty} \frac{1}{\mu\sqrt{\pi}} e^{-\frac{(R+y-R_0)^2}{2\mu^2} - 2ik_0y - \frac{(R-y-R_0)^2}{2\mu^2}} e^{\frac{2ipy}{\hbar}} dy \tag{B.5}$$

Simplifying the 2 quadratic equations (equation (B.5)) we get:

$$W(p,R) = \frac{1}{\pi\hbar}\int_{-\infty}^{\infty} \frac{1}{\mu\sqrt{\pi}} e^{-\mu^{-2}\left(y^2 - 2ik_0 y\mu^2 + (R-R_0)^2\right)} e^{\frac{2ipy}{\hbar}} dy \tag{B.6}$$

We can now take the expressions not dependant on y outside of the integral and combine the exponents.

$$W(p,R) = \frac{1}{\pi\sqrt{\pi}\mu\hbar} e^{-\frac{(R-R_0)^2}{\mu^2}} \int_{-\infty}^{\infty} e^{-\frac{y^2 + 2iy\mu^2\left(\frac{p}{\hbar} - k_0\right)}{\mu^2}} dy \tag{B.7}$$

Integrating we get:

$$\int e^{-\frac{y^2 + 2iy\mu^2\left(\frac{p}{\hbar} - k_0\right)}{\mu^2}} dy = \frac{\sqrt{\pi}\mu}{2} e^{-\frac{\mu^2}{\hbar^2}(p - \hbar k_0)^2} erf\left[\frac{y}{\mu} + i\left(\frac{p\mu}{\hbar} - \mu k_0\right)\right] \tag{B.8}$$

Applying limits we get:

$$\int_{-\infty}^{\infty} e^{-\frac{y^2 + 2iy\mu^2\left(\frac{p}{\hbar} - k_0\right)}{\mu^2}} dy = \sqrt{\pi}\mu e^{-\frac{\mu^2}{\hbar^2}(p - \hbar k_0)^2} \tag{B.9}$$

Substituting this back into the Wigner distribution (equation (B.2)) we finally get:

$$W(p,R) = \frac{1}{\pi\hbar} e^{-\frac{(R-R_0)^2}{\mu^2}} e^{-\frac{(p - \hbar k_0)^2}{\hbar^2/\mu^2}} \tag{B.10}$$

Taking the maringal integrals we get the position and velocity probability distributions:

$$|f(R)|^2 = \frac{2}{\mu\sqrt{\pi}} e^{-\frac{(R-R_0)^2}{\mu^2}} \tag{B.11}$$

$$|f(p)|^2 = \frac{2}{\frac{\hbar}{\mu}\sqrt{\pi}} e^{-\frac{\mu^2}{\hbar^2}(p - \hbar k_0)^2} \tag{B.12}$$

The above distributions are randomly sampled to get initial atomic velocities and positions for each simulation.

Appendix C

Norm Conservation in CTMQC and Ehrenfest

A statement of the conservation of the norm is given below in equation (C.1)

$$\frac{d}{dt}\sum_l |C_l(t)|^2 = \sum_l C_l^*(t)\frac{dC_l(t)}{dt} + \frac{dC_l^*(t)}{dt}C_l(t) = 0 \tag{C.1}$$

Because the adiabatic populations are real we can remove any imaginary parts.

$$\frac{d}{dt}\sum_l |C_l(t)|^2 = 2\mathbb{R}\left[C_l^*(t)\frac{dC_l(t)}{dt}\right] \tag{C.2}$$

Substituting the equation for the evolution of the adiabatic coefficients (and removing the purely imaginary term into (C.2) we get equation (C.4)

$$\frac{d}{dt}\sum_l |C_l(t)|^2 = 2\sum_l \mathbb{R}\left[\cancel{\frac{-i}{\hbar}\varepsilon_{BO}^l C_l(t)^* C_l(t)} - \sum_k C_l(t)^* C_k(t) d_{lk}^{ad} - (K^{sum} - K_l^{ad})C_l(t)^* C_l(t)\right] \tag{C.3}$$

$$= -2\sum_l \mathbb{R}\left[\sum_k C_l(t)^* C_k(t) d_{lk}^{ad} - (K^{sum} - K_l^{ad})C_l(t)^* C_l(t)\right] \tag{C.4}$$

Where:

$$K^{sum} = \sum_{\nu=1}^{N_n} \sum_{k} \frac{\mathscr{Q}_{lk,\nu}(t)}{\hbar M_\nu} \cdot |C_k(t)|^2 \mathbf{f}_{k,\nu}(t) \tag{C.5}$$

$$K_l^{ad} = \sum_{\nu=1}^{N_n} \sum_{k} \frac{\mathscr{Q}_{lk,\nu}(t)}{\hbar M_\nu} \cdot \mathbf{f}_{l,\nu}(t) \tag{C.6}$$

The NACE term evaluates to 0 due to the anti-symmetry of the NACE giving us equation (C.8).

So far, we have proved that the norm should be conserved here for all terms apart from the quantum momentum terms i.e. Ehrenfest.

$$\frac{d}{dt}\sum_l |C_l(t)|^2 = 2\sum_l \mathbb{R}\left[(K^{sum} - K_l^{ad}) C_l(t)^* C_l(t)\right] \tag{C.7}$$

$$= 2\left[K^{sum} - \sum_l K_l^{ad} |C_l(t)|^2\right] \tag{C.8}$$

However, $K^{sum} \equiv \sum_l K_l^{ad} |C_l|^2$, therefore the norm should be conserved when summed over trajectories. This statement doesn't apply to individual trajectories though, and the norm may or may not be conserved for each of them. This is because they are coupled via the quantum momentum and population may transfer between trajectories.

Appendix D

Colophon

This is a description of the tools you used to make your thesis. It helps people make future documents, reminds you, and looks good.

(example) This document was set in the Times Roman typeface using LaTeX and BibTeX, composed with the Atom text editor.

Bibliography

[1] C. K. Chiang, C. R. Fincher, Y. W. Park, A. J. Heeger, H. Shirakawa, E. J. Louis, S. C. Gau, and Alan G. MacDiarmid. Electrical Conductivity in Doped Polyacetylene. Physical Review Letters, 39(17):1098–1101, October 1977.

[2] Hideki Shirakawa, Edwin J. Louis, Alan G. MacDiarmid, Chwan K. Chiang, and Alan J. Heeger. Synthesis of electrically conducting organic polymers: halogen derivatives of polyacetylene, (CH)x. J. Chem. Soc., Chem. Commun., 0(16):578–580, Jan 1977.

[3] Bernard Kippelen and Jean-Luc Brédas. Organic photovoltaics. Energy Environ. Sci., 2(3):251–261, 2009.

[4] M. J. Małachowski and J. Żmija. Organic field-effect transistors. Opto-Electron. Rev., 18(2):121–136, Jun 2010.

[5] N. Thejo Kalyani and S. J. Dhoble. Organic light emitting diodes: Energy saving lighting technology—A review. Renewable Sustainable Energy Rev., 16(5):2696–2723, Jun 2012.

[6] Sebastian Reineke, Frank Lindner, Gregor Schwartz, Nico Seidler, Karsten Walzer, Björn Lüssem, and Karl Leo. White organic light-emitting diodes with fluorescent tube efficiency. Nature, 459(7244):234, May 2009.

[7] Kazuki Kato, Toshihiko Iwasaki, and Takatoshi Tsujimura. Over 130 lm/w all-phosphorescent white oleds for next-generation lighting. Journal of Photopolymer Science and Technology, 28:335–340, 10 2015.

[8] Veaceslav Coropceanu, Jérôme Cornil, Demetrio A. da Silva Filho, Yoann Olivier, Robert Silbey, and Jean-Luc Brédas. Charge Transport in Organic Semiconductors. Chemical Reviews, 107(4):926–952, April 2007.

[9] Samuele Giannini, Antoine Carof, Matthew Ellis, Hui Yang, Orestis George Ziogos, Soumya Ghosh, and Jochen Blumberger. Quantum localization and delocalization of charge carriers in organic semiconducting crystals. Nature Communications, 10(1):3843, Aug 2019.

[10] Alessandro Troisi. Charge transport in high mobility molecular semiconductors: classical models and new theories. Chem. Soc. Rev., 40:2347–2358, 2011.

[11] Simone Fratini, Didier Mayou, and Sergio Ciuchi. The transient localization scenario for charge transport in crystalline organic materials. Advanced Functional Materials, 26(14):2292–2315, 2016.

[12] I. Yavuz. Dichotomy between the band and hopping transport in organic crystals: insights from experiments. Physical Chemistry Chemical Physics, 19(38):25819–25828, 2017.

[13] J. S. Brown and S. E. Shaheen. Introducing correlations into carrier transport simulations of disordered materials through seeded nucleation: impact on density of states, carrier mobility, and carrier statistics. J. Phys.: Condens. Matter, 30(13):135702, Mar 2018.

[14] Tino Zimmerling and Bertram Batlogg. Improving charge injection in high-mobility rubrene crystals: From contact-limited to channel-dominated transistors. Journal of Applied Physics, 115(16):164511, 2014.

[15] V. Podzorov, E. Menard, A. Borissov, V. Kiryukhin, J. A. Rogers, and M. E. Gershenson. Intrinsic charge transport on the surface of organic semiconductors. Phys. Rev. Lett., 93:086602, Aug 2004.

[16] Samuele Giannini, Antoine Carof, and Jochen Blumberger. Crossover from Hopping to Band-Like Charge Transport in an Organic Semiconductor Model: Atomistic

Nonadiabatic Molecular Dynamics Simulation. The Journal of Physical Chemistry Letters, 9(11):3116–3123, June 2018.

[17] Harald Oberhofer, Karsten Reuter, and Jochen Blumberger. Charge Transport in Molecular Materials: An Assessment of Computational Methods. Chemical Reviews, 117(15):10319–10357, August 2017.

[18] John C. Tully. Nonadiabatic Dynamics. pages 34–71.

[19] Simone Pisana, Michele Lazzeri, Cinzia Casiraghi, Kostya S. Novoselov, A. K. Geim, Andrea C. Ferrari, and Francesco Mauri. Breakdown of the adiabatic Born–Oppenheimer approximation in graphene. Nat. Mater., 6(3):198, Feb 2007.

[20] M. Born and R. Oppenheimer. Zur Quantentheorie der Molekeln. Ann. Phys., 389(20):457–484, Jan 1927.

[21] Sharon Hammes-Schiffer. Theoretical Perspectives on Proton-Coupled Electron Transfer Reactions. Acc. Chem. Res., 34(4):273–281, Apr 2001.

[22] Sharon Hammes-Schiffer and John C. Tully. Proton transfer in solution: Molecular dynamics with quantum transitions. J. Chem. Phys., 101(6):4657–4667, Sep 1994.

[23] My Hang V. Huynh and Thomas J. Meyer. Proton-coupled electron transfer. Chemical Reviews, 107(11):5004–5064, Nov 2007.

[24] John C. Tully. Nonadiabatic molecular dynamics. International Journal of Quantum Chemistry, 40(S25):299–309, 1991.

[25] Raymond Kapral and Giovanni Ciccotti. Mixed quantum-classical dynamics. J. Chem. Phys., 110(18):8919–8929, May 1999.

[26] Todd J. Martínez∗. Insights for Light-Driven Molecular Devices from Ab Initio Multiple Spawning Excited-State Dynamics of Organic and Biological Chromophores. American Chemical Society, Oct 2005.

[27] Guillermo Albareda, Heiko Appel, Ignacio Franco, Ali Abedi, and Angel Rubio. Correlated Electron-Nuclear Dynamics with Conditional Wave Functions. Phys. Rev. Lett., 113(8):083003, Aug 2014.

[28] John C. Tully. Molecular dynamics with electronic transitions. J. Chem. Phys., 93(2):1061–1071, Jul 1990.

[29] R. L et al Whetten. Molecular dynamics beyond the adiabatic approximation: New experiments and theory. Ann. Rev. Phys. Chem., 36:277–320.

[30] Neil Shenvi, Joseph E. Subotnik, and Weitao Yang. Simultaneous-trajectory surface hopping: A parameter-free algorithm for implementing decoherence in nonadiabatic dynamics. J. Chem. Phys., 134(14):144102, Apr 2011.

[31] D. F. Coker and L. Xiao. Methods for molecular dynamics with nonadiabatic transitions. J. Chem. Phys., 102(1):496–510, Jan 1995.

[32] Joseph E. Subotnik, Amber Jain, Brian Landry, Andrew Petit, Wenjun Ouyang, and Nicole Bellonzi. Understanding the surface hopping view of electronic transitions and decoherence. Annual Review of Physical Chemistry, 67(1):387–417, 2016. PMID: 27215818.

[33] Giovanni Granucci, Maurizio Persico, and Alberto Zoccante. Including quantum decoherence in surface hopping. The Journal of Chemical Physics, 133(13):134111, 2010.

[34] Heather M. Jaeger, Sean Fischer, and Oleg V. Prezhdo. Decoherence-induced surface hopping. The Journal of Chemical Physics, 137(22):22A545, 2012.

[35] Amber Jain, Ethan Alguire, and Joseph E. Subotnik. An efficient, augmented surface hopping algorithm that includes decoherence for use in large-scale simulations. Journal of Chemical Theory and Computation, 12(11):5256–5268, Nov 2016.

[36] Joseph E. Subotnik and Neil Shenvi. A new approach to decoherence and momentum rescaling in the surface hopping algorithm. The Journal of Chemical Physics, 134(2):024105, 2011.

[37] Xiaosong Li, John C. Tully, H. Bernhard Schlegel, and Michael J. Frisch. Ab initio Ehrenfest dynamics. J. Chem. Phys., 123(8):084106, Aug 2005.

[38] Kenichiro Saita and Dmitrii V. Shalashilin. On-the-fly ab initio molecular dynamics with multiconfigurational Ehrenfest method. J. Chem. Phys., 137(22):22A506, Dec 2012.

[39] Daniela Kohen, Frank H. Stillinger, and John C. Tully. Model studies of nonadiabatic dynamics. J. Chem. Phys., 109(12):4713–4725, Sep 1998.

[40] John C. Tully. Perspective: Nonadiabatic dynamics theory. The Journal of Chemical Physics, 137(22):22A301, December 2012.

[41] Priya V. Parandekar and John C. Tully. Detailed Balance in Ehrenfest Mixed Quantum-Classical Dynamics. Journal of Chemical Theory and Computation, 2(2):229–235, March 2006.

[42] John C. Tully. Molecular dynamics with electronic transitions. The Journal of Chemical Physics, 93(2):1061–1071, July 1990.

[43] Graeme H. Gossel, Federica Agostini, and Neepa T. Maitra. Coupled-Trajectory Mixed Quantum-Classical Algorithm: A Deconstruction. Journal of Chemical Theory and Computation, August 2018.

[44] Fruzsina Gajdos, Siim Valner, Felix Hoffmann, Jacob Spencer, Marian Breuer, Adam Kubas, Michel Dupuis, and Jochen Blumberger. Ultrafast Estimation of Electronic Couplings for Electron Transfer between -Conjugated Organic Molecules. Journal of Chemical Theory and Computation, 10(10):4653–4660, October 2014.

[45] J. VandeVondele, J; Hutter. Gaussian basis sets for accurate calculations on molecular systems in gas and condensed phases. The Journal of Chemical Physics, 127(11).

[46] J. Spencer, F. Gajdos, and J. Blumberger. FOB-SH: Fragment orbital-based surface hopping for charge carrier transport in organic and biological molecules and materials. The Journal of Chemical Physics, 145(6):064102, August 2016.

[47] Antoine Carof, Samuele Giannini, and Jochen Blumberger. Detailed balance, internal consistency, and energy conservation in fragment orbital-based surface hopping. The Journal of Chemical Physics, 147(21):214113, December 2017.

[48] Biswajit Ray, Aditya G. Baradwaj, Bryan W. Boudouris, and Muhammad A. Alam. Defect characterization in organic semiconductors by forward bias capacitance–voltage (fb-cv) analysis. The Journal of Physical Chemistry C, 118(31):17461–17466, Aug 2014.

[49] W. S. Hu, Y. T. Tao, Y. J. Hsu, D. H. Wei, and Y. S. Wu. Molecular orientation of evaporated pentacene films on gold: alignment effect of self-assembled monolayer. Langmuir, 21(6):2260–2266, Mar 2005.

[50] Tatsuo Hasegawa and Jun Takeya. Organic field-effect transistors using single crystals. Science and Technology of Advanced Materials, 10(2):024314, 2009.

[51] John E. Anthony, James S. Brooks, David L. Eaton, and Sean R. Parkin. Functionalized pentacene: improved electronic properties from control of solid-state order. Journal of the American Chemical Society, 123(38):9482–9483, Sep 2001.

[52] John E. Anthony, David L. Eaton, and Sean R. Parkin. A road map to stable, soluble, easily crystallized pentacene derivatives. Organic Letters, 4(1):15–18, Jan 2002.